Matthew, J. B., Gurd, F. R. N., Garcia-Moreno, B. E., Flanagan, M. A., March, K. L., & Shire, S. J. (1985) *CRC Crit. Rev. Biochem. 18*, 91–197.
Molday, R. S., & Kallen, R. G. (1972) *J. Am. Chem. Soc. 94*, 6739–6745.
Molday, R. S., Englander, W. S., & Kallen, R. G. (1972) *Biochemistry 11*, 150–158.
Nakanishi, M., Masamichi, T., Ikegami, A., & Kanehisa, M. (1972) *J. Mol. Biol. 64*, 363–378.
Perrin, C., & Lollo, C. (1984) *J. Am. Chem. Soc. 106*, 2754–2757.
Schellman, J. A. (1955) *C. R. Trav. Lab. Carlsberg, Ser. Chim. 29*, 230–259.
Terwilliger, T. C., & Eisenberg, D. (1982) *J. Biol. Chem. 257*, 6016–6022.
Terwilliger, T. C., Weissman, L., & Eisenberg, D. (1982) *Biophys. J. 37*, 353–359.
Tuchsen, E., & Woodward, C. (1985) *J. Mol. Biol. 185*, 421–430.
Vasant Kumar, N., & Kallenbach, N. R. (1985) *Biochemistry 24*, 7658–7662.
Wagner, G., Stassinopoulou, C. I., & Wuthrich, K. (1984) *Eur. J. Biochem. 145*, 431–436.
Wand, A. J., Roder, H., & Englander, S. W. (1986) *Biochemistry 25*, 1107–1114.
Wemmer, D., & Kallenbach, N. R. (1983) *Biochemistry 22*, 1901–1906.
Woodward, C., Simon, I., & Tuchsen, E. (1982) *Mol. Cell. Biochem. 48*, 135–160.

# Nested Allosteric Interaction in Tarantula Hemocyanin Revealed through the Binding of Oxygen and Carbon Monoxide†

Heinz Decker,‡ Patrick R. Connelly,§ Charles H. Robert,§ and Stanley J. Gill*,§

*Department of Chemistry and Biochemistry, University of Colorado, Boulder, Colorado 80309-0215, and Zoologisches Institut, Universitat Munchen, 8 Munchen 2, FRG*

*Received December 17, 1987; Revised Manuscript Received April 19, 1988*

ABSTRACT: We have examined the competitive binding of oxygen and carbon monoxide to the multisubunit hemocyanin of the tarantula *Eurypelma californicum*. Employment of high-precision thin-layer methods has enabled detailed characterization of the pure oxygen and pure carbon monoxide binding curves, as well as binding curves performed under mixed-gas conditions. The pure oxygen binding curve and the displacement of oxygen by carbon monoxide at full ligand saturation are highly cooperative, but in the absence of oxygen, carbon monoxide binds noncooperatively. The results were analyzed globally within the framework of a *nested allosteric model* [Robert, C. H., Decker, H., Richey, B., Gill, S. J., & Wyman, J. (1987) *Proc. Natl. Acad. Sci. U.S.A. 84*, 1891–1895] which takes into account the hierarchy of subunit structure present in the macromolecule. The use of two ligands enables one to recognize two distinct levels of allosteric interaction functioning in the protein assembly. The binding characteristics of the allosteric states demonstrated for *Eurypelma* follow a similar pattern as those found earlier for *Homarus americanus*.

Hemocyanins are large multisubunit proteins that provide for oxygen transport in many species of arthropods and mollusks. Among the properties of hemocyanins that motivate a study of the thermodynamics of their binding reactions are the following: (1) functionally, they display highly cooperative behavior in binding oxygen (Van Holde & Miller, 1982), and (2) structurally, they reveal hierarchies of subunit organization typical of many macromolecular complexes found in biological systems (Robert et al., 1987; Wyman, 1972). In arthropods the basic structural element is a hexamer. Various species have been reported to have structures consisting of a single hexamer, a single dimerized aggregate of a hexamer (dodecamer), and higher aggregates composed of two or four dodecamers (Van Holde & Van Bruggen, 1971; van Bruggen et al., 1982; Markl, 1986). The general notion that the hierarchy of structure present in large macromolecules is reflected in a corresponding hierarchy of function through allosteric interaction was introduced by Wyman and has been termed "nesting" (Wyman, 1985, 1972). More recently, it has been described in a quantitative manner in regard to hemocyanins (Robert et al., 1987).

Among arthropod hemocyanins, that of the tarantula, *Eurypelma californicum*, has been the subject of extensive structural investigations which reveal that it has 24 subunits arranged as a dimer of isologous dodecamers (Markl et al., 1981a,b). Each dodecamer is composed of seven different types of subunits (Markl et al., 1982). In addition, the crystal structure of a closely related hexameric arthropod hemocyanin from the spiny lobster, *Panulirus interruptus*, has been determined at a resolution of 3.2 Å (Gaykema et al., 1984, 1986). The reaction of *Eurypelma* hemocyanin with oxygen is highly cooperative. Hill slopes exceeding 7 have been reported (Loewe et al., 1977; Loewe, 1978; Decker, 1981), making it one of the most cooperative of any binding system studied. In contrast to oxygen binding, carbon monoxide binds to arthropod hemocyanins noncooperatively or with only slight positive cooperativity, and with a much lower affinity than oxygen (Bonaventura et al., 1974; Brunori et al., 1981; Richey et al., 1985). Such markedly different binding behavior of

†This work was supported by National Institutes of Health Grant HL22325 (S.J.G.) and Deutsche Forschungsgesellschaft (Li 107/24-8) (H.D.).
‡Universitat Munchen.
§University of Colorado.

0006-2960/88/0427-6901$01.50/0 

oxygen and carbon monoxide makes these ligands important probes of the details concerning hemocyanin function. The two ligands bind to the same binuclear copper site of the protein in a mutually exclusive manner, with identical stoichiometry. This makes them a particularly convenient and revealing pair of ligands to study. This type of competitive, functional linkage is termed *identical linkage* (Wyman, 1964; Di Cera et al., 1987) and leads to a simplified quantitative description of the liganded species distributed in solution. Furthermore, since carbon monoxide and oxygen are both gaseous ligands, their free activities can be determined precisely, enabling a high-precision binding study.

In this paper we show that the combined use of CO and $O_2$ can lead to a detailed picture relating structure and functional aspects of this complex protein molecule. This approach has been used in exploring simple systems such as lobster hemocyanin (Richey et al., 1985) and human hemoglobin (Di Cera et al., 1987). *Eurypelma* provides an example of a protein with yet a higher level of structural organization than those previously studied in this manner.

## Theory

In order to account for the high cooperativity and marked asymmetry of the oxygen binding curve for *Eurypelma* hemocyanin, a nested model which is a generalization of the original allosteric model of Monod et al. (1965) was proposed (Decker et al., 1986; Robert et al., 1987). The model regards the dodecamer as the fundamental allosteric unit and states that there is an allosteric interaction mediated by a conformational equilibrium between two states of each dodecamer. In addition to the conformational equilibrium present within each dodecamer, the model further proposes that the dodecamers interact with one another via a conformational change involving the entire 24-mer. The idea of conformational transitions within conformational transitions is termed nesting, and the model is thus called a nested allosteric model.

The quantitative description of the mass law binding of ligands to a macromolecule is facilitated by use of the binding partition function or binding polynomial (Wyman, 1964). It is desirable when possible to have a model-independent description of the data. However, for a macromolecule with a large number of sites (in this case 24), a phenomenological description of the binding equilibria is impractical from the point of view of analyzing the data. By turning to a simplified, mechanistic description of the system, one is able to provide a quantitative description of the binding processes in a manner that is (1) tractable by data analysis and (2) appealing on the basis of the structure–function relationships it implies.

The binding polynomial is the sum of the concentrations of the various liganded species written in terms of the appropriate mass law relations. The pertinent species of the model are shown schematically in Figure 1. It may be seen that there are two overall quaternary states, R and T, as in the classical allosteric formulation of Monod et al. (1965)—the so-called MWC model. However, within each of these overall states there are two substates. The two substates nested within the R state are called Rr and Rt. These states correspond to the two different proposed equilibrium conformations of the dodecamers in the R state. Similarly, there are two substates within the T state called Tr and Tt. The dodecamers are treated as identical subunits with regard to their binding reactions. The model proposes that in the overall R state each dodecamer behaves according to an MWC description. In the overall T state, each dodecamer is also described by an MWC model. The crucial point is that the MWC descriptions of each overall state (R or T) are different.

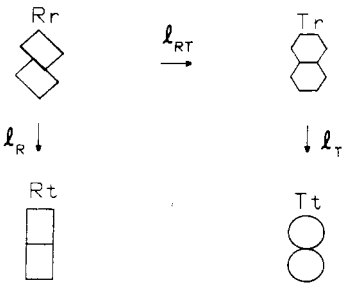


FIGURE 1: Schematic representation of the nested allosteric model for tarantula hemocyanin. Each dodecameric state is represented by a different geometric form to show that each has a particular equilibrium conformation. The equilibrium constants are given for the reactions in the directions of the arrows (see Appendix for further details).

Taking into account these features, we may formulate the following binding polynomial for oxygen binding to the tarantula hemocyanin 24-mer:

$$P_x = \nu_R P_{Rx}^2 + \nu_T P_{Tx}^2 \quad (1)$$

where $P_{Rx}$ and $P_{Tx}$ are binding polynomials for the dodecamers and the $\nu$'s are the fractions of hemocyanin in a particular conformational form when no ligand is present.

The dodecamers in a particular overall state (R or T) are described by their own binding polynomals (termed subbinding polynomials since they describe a substate of an overall state), $P_{Rx}$ and $P_{Tx}$: $P_{Rx} = \nu_{Rr}(1 + \kappa_{Rr}^{O_2}x)^{12} + \nu_{Rt}(1 + \kappa_{Rt}^{O_2}x)^{12}$ and $P_{Tx} = \nu_{Tr}(1 + \kappa_{Tr}^{O_2}x)^{12} + \nu_{Tt}(1 + \kappa_{Tt}^{O_2}x)^{12}$. In these equations, $x$ is oxygen activity and the $\kappa$'s are the equilibrium constants for the binding of oxygen to a particular conformational form indexed by the appropriate subscript (see Appendix). The fact that each subbinding polynomial is squared reflects the hypothesis that the two dodecamers bind oxygen identically and that they do not interact with one another at the level of the substate. The allosteric interaction between the dodecamers is recognized only through the equilibrium between the overall states, R and T. From the fact that each subbinding polynomial is a simple two-state allosteric polynomial and thus can produce only positive cooperativity (Monod et al., 1965), it can be shown that the entire nested polynomial can only produce positive cooperativity as well.

The binding polynomials for the mixtures of carbon monoxide and oxygen, and the detailed expressions for the amounts of the two ligands bound to hemocyanin as functions of their activities, are described in the Appendix.

## Materials and Methods

*Materials. E. californicum* hemolymph was obtained by heart puncture as described previously (Markl et al., 1980). All samples were diluted 1:1 with 0.1 M Tris buffer containing 5 mM $MgCl_2$ and 5 mM $CaCl_2$ at pH 8.0 (at 20 °C). The supernatant was centrifuged for 10 min and then dialyzed against the same buffer at 5 °C overnight. The concentration of protein used for the binding studies was 20 mg/mL as calculated from the extinction coefficient at 280 nm, $\epsilon = 1.32$ mL $mg^{-1}$ $cm^{-1}$. To ensure that ligand-induced dissociation of the protein was negligible under our solution conditions, additional $O_2$ binding experiments were performed with the same sample diluted 1:5 with buffer. The binding curves for the two concentrations were essentially identical. Previous studies with an analytical ultracentrifuge (Decker et al., 1979) confirm that the 24-mer is the stable species under the solution conditions used in this study.

*Binding Curve Measurement.* The binding curves were obtained with the thin-layer optical absorbance cell described

previously (Dolman & Gill, 1978). Four types of experiments were performed. Pure $O_2$ and CO binding curves were obtained by equilibrating the thin layer of hemocyanin with wet $O_2$ or CO at atmospheric pressure and then diluting the gas phase in contact with the solution with $N_2$. The presence of bound $O_2$ was monitored by the absorbance change at 335 nm and that of bound CO monitored by the absorbance change at 315 nm (Bonaventura et al., 1974) with a Cary 219 spectrophotometer.

In a third type of experiment, the hemocyanin solution was saturated with $O_2$, and then dilutions with CO were made to follow the competitive binding reaction. The fourth type of experiment was carried out by equilibrating the protein solution with a mixture of CO and $O_2$ of known partial pressures. Dilutions of this mixture were made with $N_2$ such that the ratio of partial pressures of CO and $O_2$ remained constant. The bound $O_2$ was monitored in these experiments by following the absorbance change at 335 nm, where there is no contribution to the spectral signal from the CO–protein complex. The remarkable stability of the thin layers of solution permitted all four types of experiments to be performed with the same layer for a given set of runs, since the base-line absorbance of the thin layer remained stable for at least 12 h. All binding curves were obtained at 25 °C. The combination of all four types of experiments allowed us to study the hemocyanin in its various stages of ligation with the two gaseous ligands. Further details of these procedures have been discussed elsewhere (Zolla et al., 1985; Di Cera et al., 1987).

*Data Analysis.* At each dilution step in an experiment, the absorbance change is computed. The observed change in absorbance for the $i$th dilution step where the ligand partial pressure changes from $p_{i-1}$ to $p_i$ is given by

$$\Delta A_i = \Delta A_T(\theta_i - \theta_{i-1}) \quad (2)$$

where $\theta$ is the fractional ligand saturation of the macromolecule at a given step (see Appendix) and $\Delta A_T$ is a fitted parameter corresponding to the optical density change between the hemocyanin in fully liganded and completely unliganded states (Gill et al., 1987). The smooth representation of this function is obtained by writing $x_{i-1} = x_i/D$, where $D$ is the dilution factor for the thin-layer device (in these experiments $D = 0.694$) and the resulting $\Delta A$ values are positioned in the middle of the $\Delta \log p_{O_2}$ interval (or $\Delta \log p_{CO}$ interval for the CO binding curve) at $\xi_i = (x_i x_{i-1})^{1/2}$. The fractional ligand saturation is equal to the amount of ligand bound per mole of hemocyanin, $\bar{X}$ for $O_2$ and $\bar{Y}$ for CO, divided by the number of binding sites, 24 (see Appendix).

All binding parameters as well as $\Delta A_T$ were estimated by least-squares regression analysis using the Gauss–Newton algorithm as modified by Marquardt (Bevington, 1969). Starting guesses for the R-state binding constants were chosen to correspond to the first and last intrinsic binding affinities of isolated dodecamers obtained from asymptotes of Hill plots of dodecameric data as reported in a previous study (Decker et al., 1986). After constrained minimization with these parameters fixed, all parameters were subsequently analyzed simultaneously.

## Results

Although the binding of a single type of ligand to a macromolecule may be described by a particular molecular model, a more stringent test of the model is provided by an examination of the binding of more than one type of ligand. In the case of respiratory proteins one often looks to the proton as an additional ligand because of its physiological significance as a regulator of oxygen binding. However, the number of proton binding sites is often not known, and the number of protons bound and free can be difficult to obtain to high precision. Such informational and operational limitations can hinder a rigorous analysis of the thermodynamics of binding.

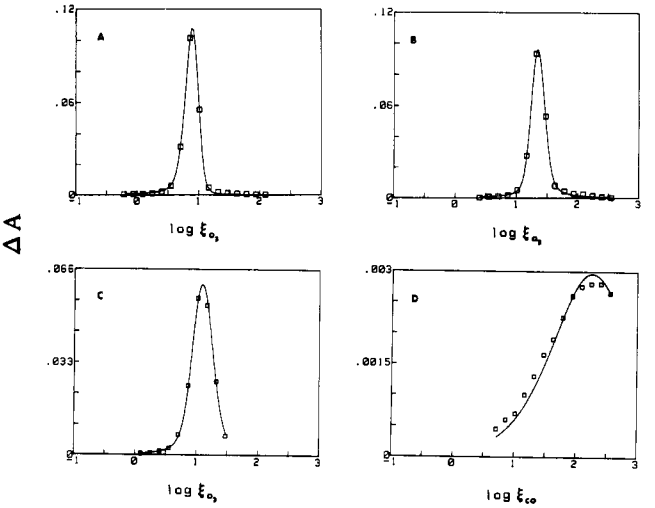


FIGURE 2: Differential binding data for the experiments outlined under Materials and Methods: (A) $O_2$ binding, (B) replacement of $O_2$ by CO, (C) displacement of ligands at constant ratio of $O_2$ to CO activities (=50.86/555.086), and (D) CO binding. Each plot records the changes in absorbance corresponding to the changes in ligand partial pressure. The titration points in each of the plots are positioned at the arithmetic mean of the logarithms of the initial and final partial pressures of oxygen (A–C) or carbon monoxide (D) for each titration step (log $\xi$). The theoretical curves are thus derivatives of the binding curves and represent the best fit upon simultaneously fitting the data sets with the model given in eq A1.

Carbon monoxide, on the other hand, is a particularly convenient ligand to study, and it can reveal important features of hemocyanin function. The stoichiometry of the CO–hemocyanin complex is known. The amount of bound carbon monoxide is easily measured by a spectroscopic signal at 315 nm (Bonaventura et al., 1974), and since carbon monoxide is a gaseous ligand, activity can be controlled to high precision. Finally, because carbon monoxide and oxygen bind to the same site in a mutually exclusive manner, the quantitative description of their binding behavior is simplified (see Appendix).

The simplifying features in the analysis and acquisition of precise binding data on both oxygen and carbon monoxide binding facilitates the testing of a particular molecular model for the binding behavior. This was especially true in the case of lobster hemocyanin in which the oxygen binding data could be described by a simple two-state MWC model, but the carbon monoxide and competitive binding data showed that the MWC model was inconsistent (Richey et al., 1985). Here we report the results of analyzing the binding of pure oxygen and carbon monoxide, and competitive binding of these ligands to tarantula hemocyanin by simultaneously fitting all of the data to the nested allosteric model outlined above.

The binding data for the four experiments outlined under Materials and Methods are shown in Figure 2 in the form of differential binding curves. These plots are the observed change in absorbance versus the logarithm of the geometric mean of the initial and final partial pressures for each step. The theoretical curves represent the best fit to the data with parameters given in Table I. A notable result is that all four experiments can be fit with the same values of the conformational equilibrium constants, $L$, $\ell_R$, and $\ell_T$, as is required in the simultaneous fitting procedure. All 11 binding parameters, as well as the total absorbance change, were allowed to vary freely in the simultaneous fit of the four data sets of

Table I: Model Parameters As Determined by Simultaneous Fit of All Four Experiments Discussed in the Text and Corresponding Confidence Intervals[a]

| | |
|---|---|
| $\kappa_{Rr}^{O_2} = 1.43 \pm 0.16$ | $\kappa_{Rr}^{CO} = 0.017 \pm 0.004$ |
| $\kappa_{Rt}^{O_2} = 0.058 \pm 0.006$ | $\kappa_{Rt}^{CO} = 0.0038 \pm 0.0001$ |
| $\kappa_{Tr}^{O_2} = 4.6 \pm 0.3$ | $\kappa_{Tr}^{CO} = 0.017 \pm 0.004$ |
| $\kappa_{Tt}^{O_2} = 0.0081 \pm 0.0018$ | $\kappa_{Tt}^{CO} = 0.0038 \pm 0.0001$ |
| $\log L = 3.7 \pm 0.3$ | |
| $\log \ell_R = 12.8 \pm 0.5$ | |
| $\log \ell_T = 20.1 \pm 0.3$ | |

[a] The errors on the parameters are twice the value of the errors estimated in the fit.

Figure 2. For practical purposes, we used the logarithms of $L$, $\ell_R$, and $\ell_T$ as fitting parameters since this led to a faster convergence. Repeat experiments on the same sample preparation (data not shown) gave parameters within the confidence intervals reported in Table I.

The analysis of the data sets was complicated by the presence of more than one minimum with comparable standard error; i.e., parameter estimates obtained upon convergence depended upon the initial parameter guesses in the regression procedure. Our final selection of parameter estimates was guided by oxygen binding studies performed on isolated dodecamers (see Materials and Methods). In those studies strong similarities between the oxygen binding data of the isolated dodecamers and the R state of the 24-mer were pointed out (Decker et al., 1986; Savel et al., 1986). On the basis of this functional similarity we selected the parameter estimates that gave R-state binding constants consistent with this observation. Although we make no claims as to the mathematical uniqueness of this set of parameter estimates, it is clear that the values of the chosen set of parameters are well resolved within the minimum obtained, describe the data to high precision, and are motivated on the basis of independent functional information concerning the isolated dodecamers.

Attempts to fit the binding data according to a simple two-state MWC model (Monod et al., 1965) with an allosteric unit size of 6, 12, or 24 sites (since these numbers correspond to numbers of sites in typical arthropod aggregates) failed. This agrees with previous investigations (Decker et al., 1983). In addition, we attempted to fit the data with a nested allosteric model which assumes that the primary level of allosteric interaction involves the individual hexamer rather than the dodecamers. This model also failed to produce an adequate description of the data. The proposal that the dodecamer unit is the primary level of interaction is consistent with structural studies which reveal that the dodecamer is the smallest repeating structural unit. The hexamers are not identical but are assembled into the dodecamer by way of a dimeric linking subunit (Markl et al., 1982).

Although other extended allosteric models have been developed (Richey et al., 1985; Van Holde & Miller, 1982) to handle the binding behavior of hemocyanins that cannot be described by the original allosteric model (Monod et al., 1965), we are motivated to pursue the nested allosteric model on the basis of the functional properties of the isolated dodecamer. Oxygen binding to the isolated dodecamer is cooperative in and of itself (Savel et al., 1986). The nested model accounts for the cooperativity of each dodecamer assembled into the 24-mer and introduces an interaction term due to the assembly of dodecamers that is accounted for by an overall allosteric transition. It is entirely possible that more complex nested mechanisms may be operating in this molecule as suggested by the findings of Savel et al. (1986). However, these more complex nested descriptions are beyond the limits of practical analysis of this data alone. In any case, our particular choice of model must ultimately be tested by other means including suitable probes of structural details.

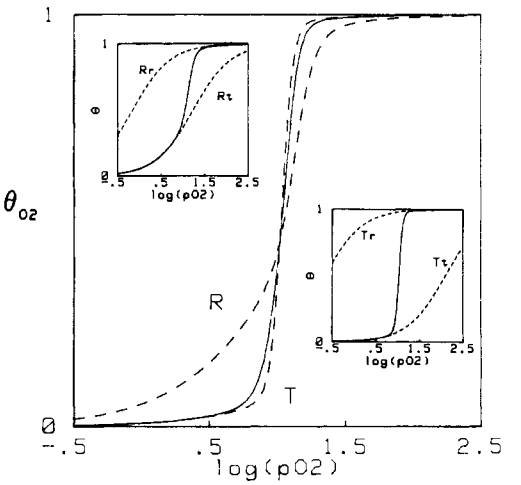


FIGURE 3: Pure oxygen binding curves generated from best fit model parameters (see Table I) for the R state and T states alone (---), and the entire binding process (—). The solid line shows the sharp transition from the T to the R state that accompanies oxygenation. Upper left inset: Binding curves for the Rr and Rt substates alone (---) and the entire R state (solid lines). Lower right inset: Binding curves for the Tr and Tt substates alone (---) and the entire T state (solid lines).

## Discussion

In order to characterize the important reactions of tarantula hemocyanin with oxygen and carbon monoxide, we consider three extreme reactions separately: (1) the oxygen reaction, $Hc + 24O_2 = Hc(O_2)_{24}$; (2) the carbon monoxide reaction, $Hc + 24CO = Hc(CO)_{24}$; and (3) the competitive displacement reaction at full total ligand saturation, $Hc(CO)_{24} + 24O_2 = Hc(O_2)_{24} + 24CO$. From the description of the data given by the model of eq A1 (see Appendix) with the best fit parameters, we generate the binding curves for each of these reaction processes.

Figure 3 shows the binding curve for the reaction with oxygen. The dashed lines in this figure show the calculated binding curves of the overall R and T states. The binding curves for the R and T states are both cooperative. The T state shows greater cooperativity than the actual binding curve, whereas the R state is less cooperative than the overall binding curve. The figure shows the sharp transition from the T to the R state that accompanies oxygenation. Likewise, the insets of Figure 3 shows the transitions among substates within each overall state, i.e., Rr to Rt and Tr to Tt. The fact that the binding curves for the R and T states nearly overlap at high oxygen saturation but diverge at lower saturation suggests that the Rr and Tr states a more alike than the Rt and Tt states.

Upon comparison of the oxygen binding curve obtained here with that of previous studies (Decker et al., 1986), a difference in the cooperativity is noted, particularly at low oxygen saturations. The conditions used in the present studies were chosen to match physiological conditions (Schartau & Leidescher, 1983). The increased steepness of the present oxygen binding curve in the region of low saturations is reflected in the parameters describing the different allosteric states. As one would expect, the R-state binding constants do not change far from the values determined earlier, but the binding constants of the T state (which predominates at low oxygen saturations) and the overall allosteric constant, $L$, are different. The fact that $L$ is larger reflects the increased cooperativity

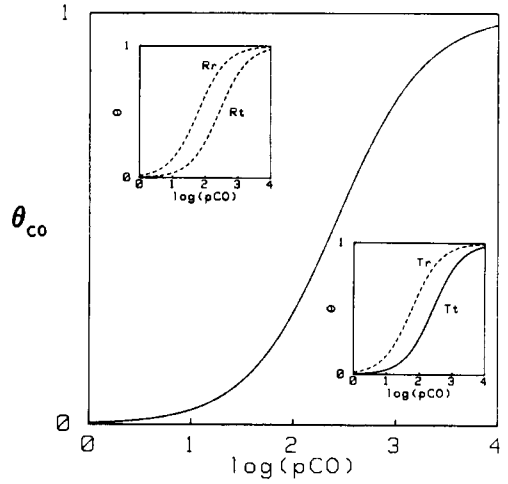


FIGURE 4: Pure carbon monoxide binding curves generated from best fit model parameters (see Table I) for the R state alone, T state alone, and entire CO binding process. Only one curve is seen because all three processes produce the same binding curves. This illustrates that the protein remains in the Tt state throughout the range of saturation and that the Rt and Tt states have the same affinities for CO as do the Tr and Rr states. The separate CO binding curves for the R states and T states are shown in the upper left and lower right insets, respectively, as was done for $O_2$ binding in Figure 3.

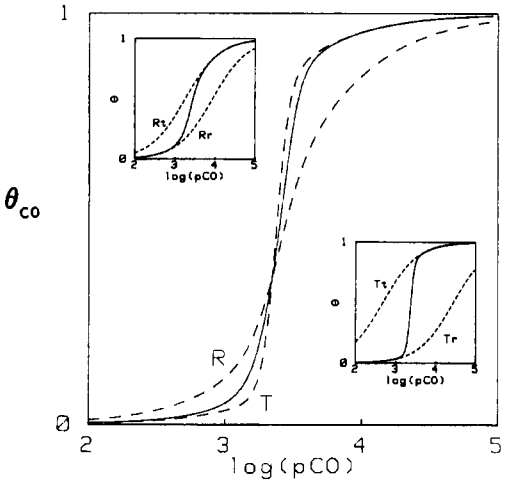


FIGURE 5: Carbon monoxide binding curves at a constant oxygen activity, $x$ = 100 Torr. At low carbon monoxide activity with 100 Torr oxygen present, the Tr and the Rr substates are most populated. As carbon monoxide activity increases, transitions to the Tt and Rt states take place.

found under the conditions employed in this study. This difference in the cooperativity is presumably due to the increased divalent cation concentrations, a result consistent with the general role that divalent cations play as heterotropic effectors of oxygen binding in arthropod hemocyanins (Miller & van Holde, 1982). In addition, chloride ion effects have been seen in some hemocyanin systems also (Brouwer et al., 1977).

The noncooperative behavior displayed by carbon monoxide stands in contrast to that of oxygen. Figure 4 shows the carbon monoxide binding curve. The molecule remains in the Tt state throughout the entire saturation range. How then can we study the carbon monoxide reactions of the hemocyanin in all four of its functional allosteric states? To do this, we must study the binding of carbon monoxide when oxygen present. Oxygen shifts the allosteric equilibrium toward states that would remain unpopulated in the presence of pure carbon monoxide. The experiments depicted in Figure 2c,d accomplished this task.

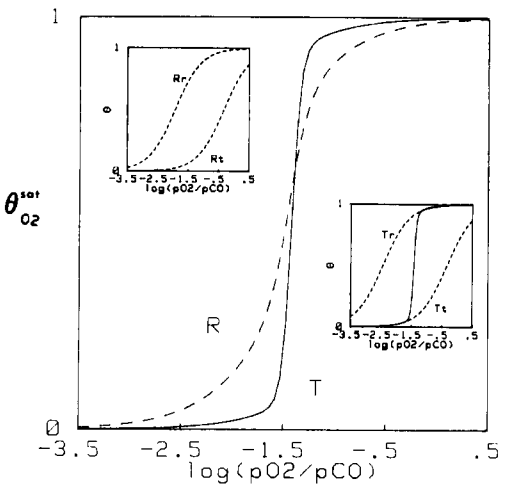


FIGURE 6: Binding curves generated from the best fit model parameters for the cooperative replacement reaction of CO by $O_2$ at full ligand saturation for R state (---), T state (---), and entire binding process (—). The replacement binding curves for the R and T states are shown in the upper left and lower right insets, respectively, as was done in Figure 3 and 4 for pure $O_2$ and pure CO. $\theta^{sat}_{O_2}$ is the oxygen saturation for the replacement binding process as defined in the Appendix.

Table II: Ratios of the Model CO to $O_2$ Association Constants for *E. californicum* and *H. americanus* Hemocyanins[a]

| | *Eurypelma* | *Homarus* | | *Eurypelma* | *Homarus* |
|---|---|---|---|---|---|
| $K^{O_2}_{Tf}/K^{CO}_{Tt}$ | 0.48 | 0.29 | $K^{O_2}_{Rf}/K^{CO}_{Rt}$ | 0.07 | 0.16 |
| $K^{O_2}_{Tf}/K^{CO}_{Tr}$ | 0.001 | 0.016 | $K^{O_2}_{Rf}/K^{CO}_{Rr}$ | 0.01 | 0.02 |

[a] The data for *Homarus* are taken from Robert et al. (1987).

To illustrate the effect that oxygen has on the carbon monoxide reaction, we may examine the carbon monoxide binding curve in the presence of a fixed amount of oxygen (Figure 5). At low carbon monoxide saturation with 100 Torr oxygen present, the Tr and the Rr states are the most populated of the allosteric states. Since carbon monoxide binding postulates the Tt and Rt states, the transition to these states occurs upon increasing the amount of carbon monoxide. This process produces highly cooperative carbon monoxide binding curves, although the molecular mechanism underlying this cooperativity is actually due to the removal of oxygen from the copper site.

The competitive binding reaction process is illustrated by the displacement of carbon monoxide by oxygen at full saturation. From the binding curve analysis given in Figure 6 we can see that only two of the four allosteric states are populated since a transition is seen only between the two T states. Although the binding curves depicted in Figures 5 and 6 are obtained only by performing experiments under pressures greater than atmospheric, it illustrates the manner in which oxygen populates states that remain unpopulated with pure carbon monoxide present. Since the competitive binding experiments reported here (Figure 2c,d) allowed us to study carbon monoxide binding to the states that were not accessed by the pure carbon monoxide reaction, the equilibrium constants for CO binding to each of the states could be resolved.

As noted above, the Rr and Tr states appear to bind oxygen similarly, whereas these states as well as the Rt and Tt states bind carbon monoxide similarly. This is borne out by the values in Table I. Examining the ratio of carbon monoxide to oxygen constants for each state furthers the comparison of the nature of each of the states. The ratios given in Table II indicate that the Tt state has the most similar affinities for the two ligands and that the Tr state has the most disparate affinities for them. The remaining two states, Rt and Rr, have

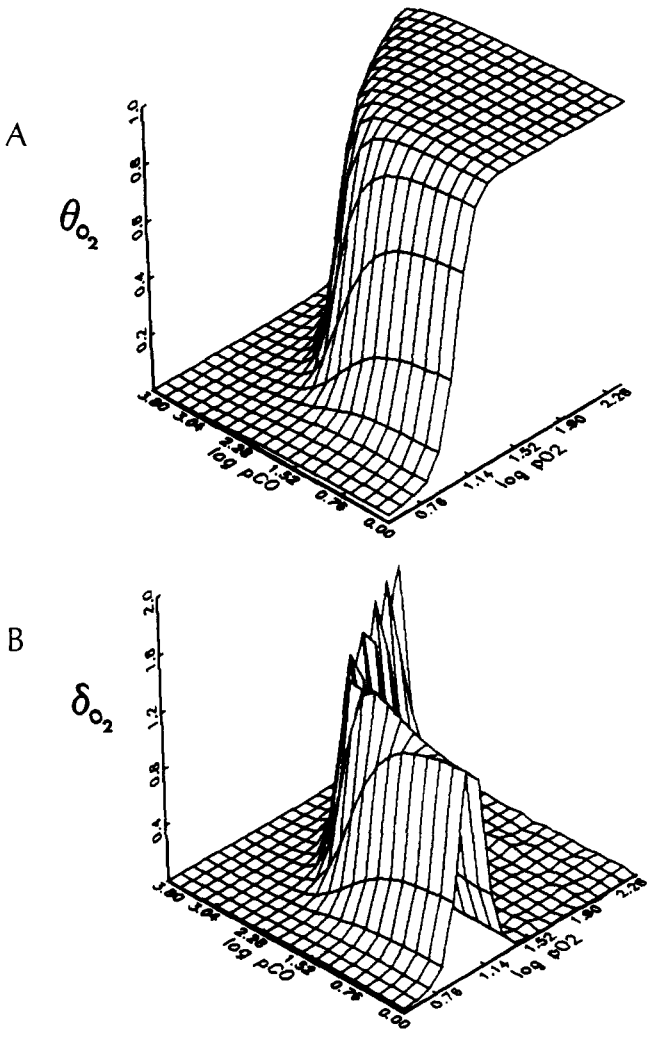


FIGURE 7: Binding surface plots of oxygen saturation, $\theta_{O_2}$, versus the logarithms of the partial pressures of oxygen and carbon monoxide (A) and the derivative of the saturation surface, $\delta_{O_2}$ (B).

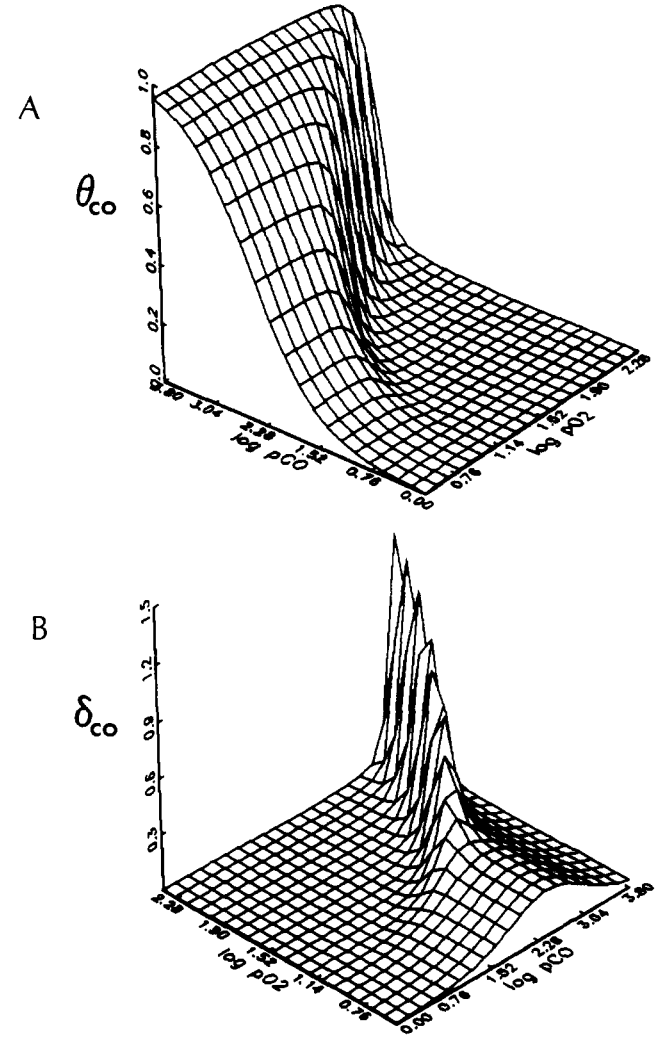


FIGURE 8: Binding surface plots of carbon monoxide saturation, $\theta_{CO}$, versus the logarithms of the partial pressures of oxygen and carbon monoxide (A) and the derivative surface, $\delta_{CO}$ (B).

similar ratios. This trend in the ratios may be compared to those of the lobster *Homarus americanus* hemocyanin studied under similar conditions (Richey et al., 1985). This hemocyanin is also from an arthropod, but its stable aggregation state is a dodecamer. Robert et al. (1987) have shown that a similar nested allosteric model explains the binding data for this species. The proposed model assumes that hexamers are nested inside the dodecamer in contrast to the proposal for the *Eurypelma* system that dodecamers are nested inside a 24-mer. Note from Table II that the same trend in the CO to $O_2$ affinity ratios is evident. This might be expected in light of the striking structural similarities of these two hemocyanins (Linzen et al., 1985) and further emphasizes the common structure–function relationships of these proteins.

A comprehensive representation of the functional properties of tarantula hemocyanin comes by considering the saturation of oxygen or carbon monoxide extended along the coordinates comprised of the activities of both ligands (Figures 7 and 8). A comparison of the derivatives of the $O_2$ and CO binding surfaces (Figures 7B and 8B) emphasizes the drastic cooperativity of pure oxygen versus pure carbon monoxide binding, indicated by the sharpness of the peak in Figure 7B as compared to the shallow hump in Figure 8B. A structural explanation for the difference in the cooperativities of CO and $O_2$ stems from the fact that CO does not bridge the two Cu ions that make up the binding site (Fagar & Alban, 1972), whereas $O_2$ forms a bridge by entering into a peroxo-Cu(II)$_2$ complex (Freedman et al., 1976). In addition, the surfaces show the competitive nature of the binding between oxygen and carbon monoxide. This can be seen from the fact that the position of the oxygen binding curve (i.e., the position of a single contour of the surface in Figure 7 at constant log $p_{CO}$) at higher activities of carbon monoxide shifts to *higher* activities of oxygen.

In conclusion, the results reported here demonstrate the binding behavior of oxygen and carbon monoxide with tarantula hemocyanin. A particularly striking result is that the replacement of oxygen by carbon monoxide at full ligand saturation is a cooperative reaction. This rests in contrast to the noncooperative replacement reaction of $O_2$ and CO in human hemoglobin (Wyman et al., 1981; Di Cera et al., 1987). The results of all the binding experiments were described by a nested allosteric model that correlates the structural and functional properties of native *Eurypelma* hemocyanin. The use of an identically linked pair of ligands, which bind in a markedly different manner, allowed a comprehensive exploration of the function of the macromolecule in each of its allosteric states. The comparison of carbon monoxide to oxygen affinity ratios of *Eurypelma* hemocyanin to those of *H. americanus* reveals a similarity in the allosteric control in these arthropod hemocyanins.

ACKNOWLEDGMENTS

We thank B. Linzen for his criticism and discussion.

## APPENDIX

In this appendix we outline the expressions needed to analyze the binding data and generate the binding curves reported in this paper.

Equation 1 under Theory gives the binding polynomial for oxygen binding. The binding polynomial for the system composed of both oxygen and carbon monoxide, $P_{xy}$, is

$$P_{xy} = \nu_R[\nu_{Rr}(1 + \kappa_{Rr}^{O_2}x + \kappa_{Rr}^{CO}y)^{12} + \nu_{Rt}(1 + \kappa_{Rt}^{O_2}x + \kappa_{Rt}^{CO}y)^{12}]^2 + \nu_T[\nu_{Tr}(1 + \kappa_{Tr}^{O_2}x + \kappa_{Tr}^{CO}y)^{12} + \nu_{Tt}(1 + \kappa_{Tt}^{O_2}x + \kappa_{Tt}^{CO}y)^{12}]^2 \quad \text{(A1)}$$

In this equation $x$ and $y$ are the activities of oxygen and carbon monoxide respectively, the $\nu$'s are the fractions of each allosteric state, and the $\kappa$'s are the equilibrium constants for ligand binding to each allosteric state. The fact that there are no cross terms ($xy$ terms) in $P_{xy}$ reflects the special nature of the linkage between these two ligands. It rules out the possibility that a single binding site may bind both $O_2$ and CO simultaneously. This feature, termed *identical linkage* (Wyman, 1964), has been demonstrated for both arthropod (Richey et al., 1985) and molluscan (Zolla et al., 1985) hemocyanins.

There are six terms that are common to $P_x$ and $P_{xy}$. They are the fractions of the proposed states in the absence of ligand: $\nu_R$ and the fractions of its substates $\nu_{Rr}$ and $\nu_{Rt}$; and $\nu_T$ along with the fractions of its substates $\nu_{Tr}$ and $\nu_{Tt}$. These terms may be expressed in terms of three equilibrium constants:

$$\nu_R = \frac{1}{1 + L} \qquad \nu_T = \frac{L}{1 + L} \quad \text{(A2)}$$

$$\nu_{Rr} = \frac{1}{1 + \ell_R} \qquad \nu_{Tr} = \frac{1}{1 + \ell_T} \quad \text{(A3)}$$

$$\nu_{Rt} = \frac{\ell_R}{1 + \ell_R} \qquad \nu_{Tt} = \frac{\ell_T}{1 + \ell_T} \quad \text{(A4)}$$

where $L$ is the equilibrium constant for the reaction in which the unligated R state of the macromolecule goes to the unligated T state and $\ell_R$ and $\ell_T$ are the equilibrium constants for the reactions in which the unligated Rr state and Tr state go to the unligated Rt state and Tt state, respectively. We could also designate the equilibrium constant for the reaction of the unligated Rr state going to the unligated Tr state as $\ell_{RT}$ (see Figure 1). In this case the dependency relation among the constants is $L = \ell_{RT}(1 + \ell_T)/(1 + \ell_R)$. Since any of these equilibrium constants is independent of the ligand under investigation, the binding data for $O_2$ and CO should be consistent with respect to these constants if the model is acceptable.

In order to formulate the model in terms that correspond to the experimental observables, we need expressions for the amounts of $O_2$ and CO bound as functions of the partial pressures of the ligands, for the particular reaction under investigation. These quantities can be given in terms of the binding polynomial, $P_{xy}$, for reactions of hemocyanin with $O_2$ ($M + iX \rightarrow MX_i$) and CO ($M + jY \rightarrow MY_j$), respectively, as follows:

$$\bar{X} = \left(\frac{\partial \ln P_{xy}}{\partial \ln x}\right)_y \qquad \bar{Y} = \left(\frac{\partial \ln P_{xy}}{\partial \ln y}\right)_x \quad \text{(A5)}$$

To examine these quantities for a particular state, it is necessary only to substitute the binding polynomial for that state into the expressions given in eq A5. The derivatives of these quantities are related to the differential measurements performed in this study (see Materials and Methods) and give a measure of the cooperativity of binding. For the nested model employed here, only positive cooperativity is predicted for any choice of constants.

A reaction of particular interest is the replacement of CO by $O_2$ when the molecule is fully saturated with ligand [$MY_t + iY \rightarrow MY_{t-i}X_i + (t - i)X$]. The amount of oxygen bound at any stage of this reaction is given by

$$\bar{X}^{sat} = \left(\frac{\partial \ln P_{xy}^{sat}}{\partial \ln z}\right) \quad \text{(A6)}$$

where $P^{sat} = \nu_R[\nu_{Rr}(1 + \kappa_{Rr}^{O_2}z/\kappa_{Rr}^{CO})^{12} + \nu_{Rt}(1 + \kappa_{Rt}^{O_2}z/\kappa_{Rt}^{CO})^{12}]^2 + \nu_T[\nu_{Tr}(1 + \kappa_{Tr}^{O_2}z/\kappa_{Tr}^{CO})^{12} + \nu_{Tt}(1 + \kappa_{Tt}^{O_2}z/\kappa_{Tt}^{CO})^{12}]^2$. $\bar{Y}^{sat}$ is equal to $(t - \bar{X}^{sat})$, where $z = x/y$ and $t = 24$, the number of binding sites. $\theta_{O_2}^{sat}$ is equal to $\bar{X}^{sat}$ divided by 24. The form of this binding polynomial ensures that the derivative on the right-hand side of eq A6 is carried out with the total saturation (i.e., amount of oxygen bound plus amount of carbon monoxide bound) of the macromolecule fixed at full saturation.

**Registry No.** $O_2$, 7782-44-7; CO, 630-08-0.

## REFERENCES


Bevington, P. R. (1969) *Data Analysis and Data Reduction in the Physical Sciences*, p 236, McGraw-Hill, New York.

Bonaventura, C., Sulliven, B., Boneventura, J., & Bourne, S. (1974) *Biochemistry 13*, 4784–4789.

Brouwer, M., Bonaventura, C., & Bonaventura, J. (1977) *Biochemistry 16*, 3897–3902.

Brunori, M., Zolla, L., Kuiper, H. S., & Argo, A. F. (1981) *J. Mol. Biol. 153*, 1111–1123.

Decker, H. (1981) Dissertation, University of Munich, FRG.

Decker, H., Markl, J., Loewe, R., & Linzen, B. (1979) *Hoppe-Seyler's Z. Physiol. Chem. 360*, 1505–1507.

Decker, H., Schmid, R., Markl, J., & Linzen, B. (1980) *Hoppe-Seyler's Z. Physiol. Chem. 360*, 1707–1717.

Decker, H., Savel, A., Linzen, B., & Von Holde, K. E. (1983) in *Life Chemistry Reports Supplement 1: Structure and Function in Invertebrate Respiratory Proteins* (Wood, E. J., Ed.) pp 251–256, Harwood Academic, Chur, Switzerland.

Decker, H., Robert, C. H., & Gill, S. J. (1986) in *Invertebrate Oxygen Carriers* (Linzen, B., Ed.) pp 383–388, Springer-Verlag, Berlin and Heidelberg.

Di Cera, E., Doyle, M., Connelly, P. R., & Gill, S. J. (1987) *Biochemistry 26*, 6494–6502.

Dolman, D., & Gill, S. J. (1978) *Anal. Biochem. 87*, 127–134.

Fagar, L. Y., & Alban, J. O. (1972) *Biochemistry 11*, 4786–4792.

Freedman, T. B., Loehr, J. S., & Loehr, T. M. (1976) *J. Am. Chem. Soc. 98*, 2809–2815.

Gaykema, W. P. J., Hol, W. G. J., Vergijen, J. M., Soeter, N. M., Bak, H. J., & Beintema, J. J. (1984) *Nature (London) 309*, 23–29.

Gaykema, W. P. J., Volbeda, A., & Hol, W. J. G. J. (1986) *J. Mol. Biol. 187*, 255–275.

Gill, S. J., Di Cera, E., Doyle, M. L., Bishop, G. A., & Robert, C. H. (1987) *Biochemistry 26*, 3995–4002.

Linzen, B., Soeter, N. M., Riggs, A. F., Schneider, H. J., Schartau, W., Moore, M. D., Yokata, E., Behrens, P. Q., Nakashima, N., Takagi, T., Nemoto, T., Vereijken, J. M., Bak, H. J., Beintema, J. J., Volbeda, A., Gaykema, P. J., & Hol, W. G. J. (1985) *Science (Washington, D.C.) 229*, 519–524.

Loewe, R. (1978) *J. Comp. Physiol. 128*, 161-168.
Loewe, R., Schmid, R., & Linzen, B. (1977) in *Proceedings in Life Sciences: Structure and Function of Haemocyanin* (Bannister, J. V., Ed.) pp 50-54, Springer-Verlag, Berlin and Heidelberg.
Markl, J. (1986) *Biol. Bull. (Woods Hole, Mass.) 171*, 90-115.
Markl, J., Savel, A., Decker, H., & Linzen, B. (1980) *Hoppe-Seyler's Z. Physiol. Chem. 361*, 649-660.
Markl, J., Kempter, B., Linzen, B., Bijlholt, M. M. C., & Van Bruggen, E. F. J. (1981a) *Hoppe-Seyler's Z. Physiol. Chem. 362*, 1631-1641.
Markl, J., Savel, A., & Linzen, B. (1981b) *Hoppe-Seyler's Z. Physiol. Chem. 362*, 1255-1262.
Markl, J., Decker, H., Linzen, B., Schutter, W. G., & Van Bruggen, E. F. J. (1982) *Hoppe-Seyler's Z. Physiol. Chem. 363*, 73-87.
Monod, J., Wyman, J., & Changeux, J. P. (1965) *J. Mol. Biol. 12*, 88-112.
Richey, B., Decker, H., & Gill, S. J. (1985) *Biochemistry 24*, 109-117.
Robert, C. H., Decker, H., Richey, B., Gill, S. J., & Wyman, J. (1987) *Proc. Natl. Acad. Sci. U.S.A. 84*, 1891-1895.
Savel, A., Markl, J., & Linzen, B. (1986) in *Invertebrate Oxygen Carriers* (Linzen, B., Ed.) pp 399-402, Springer-Verlag, Berlin and Heidelberg.
Schartau, W., & Leidescher, T. (1983) *J.* Comp. *Physiol. 152*, 73-77.
Van Bruggen, E. F. J., Schutter, W. G., Jan, F. L., Van Breemen, J., Bijlholt, M. M. C., & Wichertjes, T. (1982) in *Electron Microscopy of Proteins* (Harris, J. R., Ed.) Vol. 1, pp 1-38, Academic, London.
Van Holde, K. E., & Van Bruggen, E. F. J. (1971) in *Subunits in Biological Systems* (Timmasheff, S. N., & Fasman, G. D., Eds.) pp 1-53, Marcel Dekker, New York.
Van Holde, K. E., & Miller, K. (1982) *Q. Rev. Biophys. 15*, 1-129.
Wyman, J. (1964) *Adv.* Protein *Chem. 19*, 223-286.
Wyman, J. (1972) *Curr. Top. Cell. Regul. 6*, 207-223.
Wyman, J. (1984) *Q. Rev. Biophys. 17*, 453-488.
Zolla, L., Brunori, M., Richey, B., & Gill, S. J. (1985) *Biophys. Chem. 22*, 271-280.

# Dynamics Simulation Studies of Apoazurin of *Alcaligenes denitrificans*†

Lin X.-Q. Chen,‡,§ Richard A. Engh,‡,∥ Axel T. Brünger,⊥ Dzung T. Nguyen,⊥ Martin Karplus,*,⊥ and Graham R. Fleming*,‡,#

*Department of Chemistry, Harvard University, Cambridge, Massachusetts 02138, and Department of Chemistry and James Franck Institute, The University of Chicago, Chicago, Illinois 60637*

*Received December 21, 1987; Revised Manuscript Received April 28, 1988*

ABSTRACT: Molecular dynamics simulations using the stochastic boundary method were carried out for apoazurin of *Alcaligenes denitrificans*. For a region centered on the exposed tryptophyl residue (W118), simulations in vacuo and with inclusion of model water molecules were carried out. The simulations are in accord with the experimental finding that the interior tryptophan (W48) is less mobile than the exterior tryptophan (W118). In simulations with and without solvent the motion of W118 is strongly correlated with residues connected along the backbone and residues close to the face of the indole ring. The 50-ps simulated tryptophan fluorescence anisotropies did not reveal the slowly decaying component (160 ps) found experimentally. Estimates of energy transfer between W48 and W118 give rates similar to the experimental value provided that the initial state is $^1L_b$. Variations of rate of ±20% are found when the relative motions of the two residues are taken into account.

The internal motions of protein molecules have generated much interest in recent years because of their possible significance in protein function (Gurd & Rothgeb, 1979; Williams, 1979; Karplus & McCammon, 1981, 1983). A variety of techniques for the study of protein dynamics have been developed including high-resolution X-ray diffraction (Petsko & Ringe, 1984; Debrunner & Frauenfelder, 1982; Artymiuk et al., 1979), NMR (Richarz et al., 1980; Gall et al., 1981, 1982; Rice et al., 1981; Dobson & Karplus, 1986), time-resolved optical spectroscopy (Hochstrasser & Negus, 1984; Lakowicz et al., 1983; Munro et al., 1979; Petrich et al., 1987), and molecular dynamics (MD) computer simulation (Karplus & McCammon, 1981, 1983; van Gunsteren & Karplus, 1982; Ichiye & Karplus, 1983). Improvements in time-resolved spectroscopy and computers are extending the time scale of both experiment and theory, so that direct comparisons should be possible in the near future; i.e., subnanosecond events may be measured by spectroscopic methods, and molecular dynamics simulations have been extended into the nanosecond time scale. The information concerning the atomic motions provided by MD simulations can assist in the interpretation of experimental results, and the reliability of both the experimental and theoretical techniques can be tested by appropriate comparisons. It has been shown, for example, that the standard interpretation of the temperature factors in the X-ray analysis of proteins can result in significant errors in the estimates of side-chain motions (Yu et al., 1985; Kuriyan et al., 1986). The validity of the interpretation of NMR

† This work was supported by a grant from the National Science Foundation (to G.R.F. and M.K.). We also thank the National Science Foundation for the computation time on CRAY-1 and CRAY-2 supercomputers and the service provided by University of Minnesota Supercomputer Center. The Evans & Sutherland graphic system PS300 was provided by NSF Grant PCM-8304504.
‡ The University of Chicago.
§ Present address: Department of Chemistry, University of California at Berkeley, Berkeley, CA 94720.
∥ Present address: Max-Planck-Institut für Biochemie, D-8033 Martinsreid bei München, West Germany.
⊥ Harvard University.
# John Simon Guggenheim Fellow.

0006-2960/88/0427-6908$01.50/0 